Geosci. Model Dev. Discuss., 6, 3241–3287, 2013
www.geosci-model-dev-discuss.net/6/3241/2013/
doi:10.5194/gmdd-6-3241-2013

Geoscientific Model Development Discussions
Open Access

Scheme for calculation of multi-layer cloudiness and precipitation for climate models of intermediate complexity

A. V. Eliseev[1,2,3], D. Coumou[2], A. V. Chernokulsky[1], V. Petoukhov[2], and S. Petri[2]

[1]A.M. Obukhov Institute of Atmospheric Physics RAS, Moscow, Russia
[2]Potsdam Institute for Climate Impact Research, Potsdam, Germany
[3]Institute of Ecology and Geography, Kazan Federal University, Kazan, Russia

Received: 22 April 2013 – Accepted: 17 May 2013 – Published: 17 June 2013

Correspondence to: A. V. Eliseev (eliseev@ifaran.ru)

Published by Copernicus Publications on behalf of the European Geosciences Union.

Abstract

In this study we present a scheme for calculating the characteristics of multi-layer cloudiness and precipitation for climate models of intermediate complexity (EMICs). This scheme considers three-layer stratiform cloudiness and single column convective clouds. It distinguishes between ice and droplet clouds as well. Precipitation is calculated by using cloud life time, which depends on cloud type and phase as well as on statistics of synoptic and convective disturbances. The scheme is tuned to observations by using an ensemble simulation forced by the ERA-40-derived climatology for 1979–2001. Upon calibration, the scheme realistically reproduces basic features of fields of cloud amounts, cloud water path, and precipitation. The simulated globally and annually averaged total cloud amount is 0.59, and the simulated globally averaged annual precipitation is 109 $\mathrm{cm\,yr^{-1}}$. Both values agree with empirically-derived values. Geographical distribution and seasonal changes of calculated variables are broadly realistic as well. However, some important regional biases still remain in the scheme.

1 Introduction

Clouds are an important part of the climate system, linking hydrological processes with radiative transfer and atmospheric dynamics. Since the mid-1990s, climate models include prognostic cloud schemes calculating cloud amounts and cloud water content (Solomon et al., 2007; Zhang et al., 2005; Williams and Tselioudis, 2007). While such schemes are quite elaborate in the state-of-the-art models, some unresolved problems remain (Stephens, 2005; Williams and Tselioudis, 2007; Cesana and Chepfer, 2012). In particular, there is ample evidence that uncertainty in cloud response to external, e.g. anthropogenic forcing constitutes the largest part of the overall uncertainty in respective response of global climate models (Stephens, 2005; Bony et al., 2006; Dufresne and Bony, 2008; Soden and Vecchi, 2011).

For Earth system models of intermediate complexity (EMICs) (Claussen et al., 2002; Petoukhov et al., 2005; Zickfeld et al., 2013; Eby et al., 2013) this problem is even more actual. Most models of this type contain quite simplified cloudiness schemes, frequently accounting only for effective single-layer clouds (see, e.g. Table of EMICs at http://www.pik-potsdam.de/emics/toe_05-06-07.pdf). Such an approach obviously precludes to resolve dominant influence of upper-level clouds on long-wave radiative transfer in the atmosphere, and low-level clouds on the respective short-wave transfer (Stephens, 1978; Liou, 2002). In addition, from simulations with general circulation models it is expected that global warming is accompanied by smaller (larger) cloud amounts in the lower (upper) troposphere (e.g. Solomon et al., 2007). Accounting only for single-layer clouds makes it difficult for simplified climate models to reproduce these changes in cloud amounts. Further, one-layer cloud schemes are may provide only limited representation of aerosol–clouds interaction (first and second aerosol indirect effects related to changes in cloud albedo and life time correspondingly; both effects results from an impact of hydroscopic aerosols on the size of clouds droplets and ice crystals, e.g. Charlson et al., 1992; Solomon et al., 2007).

Among EMICs which currently have an effective single-layer cloudiness scheme are the models developed at the Potsdam Institute for Climate Impacts Research (Climber-2, Petoukhov et al., 2000; Ganopolski et al., 2001, and Climber-3α, Montoya et al., 2005) and at the A. M. Obukhov Institute of Atmospheric Physics, Russian Academy of Sciences IAP RAS CM, see Mokhov and Eliseev (2012). Currently, both institutes develop new versions of the EMICs (Coumou et al., 2011; Eliseev et al., 2011). As a part of this program, we are working out a new cloud-precipitation scheme. This scheme describes 3-layer stratiform clouds and one effective type of convection clouds.

In the present paper, the current version of the scheme is described and tested off-line for the present-day climate.

GMDD
6, 3241–3287, 2013

2 Governing equations

The developed scheme considers four cloud types within a given grid cell. The first three cloud types describe low-level, mid-level, and upper-level stratiform clouds (thereafter denoted with the subscripts sl, sm, and sh respectively). This distinction corresponds to observational experience at large horizontal scales (Tian and Curry, 1989; Mazin and Khrgian, 1989). The fourth cloud type is denoted by subscript co and represents convective (cumulus) clouds.

Values of basic variables are listed in Table 1.

2.1 Cloud vertical boundaries and extent

In the current set up, heights of stratiform cloud bases are related either to the height of the planetary boundary layer H_{PBL}, or to the height of the equivalent barotropic level H_{EBL}, or to the height of the tropopause H_{trop} (Petoukhov et al., 1998, 2003):

$$\begin{aligned} H_{\mathrm{b,sl}} &= C_{H,\mathrm{sl}} \cdot H_{\mathrm{PBL}}, \\ H_{\mathrm{b,sm}} &= C_{H,\mathrm{sm}} \cdot H_{\mathrm{EBL}}, \\ H_{\mathrm{b,sh}} &= C_{H,\mathrm{sh}} \cdot H_{\mathrm{trop}}, \end{aligned} \tag{1}$$

where $C_{H,\mathrm{sl}}$, $C_{H,\mathrm{sm}}$, and $C_{H,\mathrm{sh}}$ are parameters.

Calculation of geometric thickness of stratiform clouds is similar to that used in Petoukhov et al. (2000):

$$h_j = h_{j,0} c_j^{c_\mathrm{h}} \cdot F_{\mathrm{h},T,j}. \tag{2}$$

Hereafter $j \in \{\mathrm{sl}, \mathrm{sm}, \mathrm{sh}\}$ stands for cloud type, parameter $h_{j,0}$ depends on this type, c_h is constant, and dependence on temperature is

$$F_{\mathrm{h},T,j} = \exp\left(-C_{\mathrm{h,s},k} \left| T_j - C_{\mathrm{h,s},m} \right|\right). \tag{3}$$

GMDD
6, 3241–3287, 2013

Here $C_{h,s,k}$ and $C_{h,s,m}$ are constants. Cloud temperature T_j is currently assigned to the respective value at cloud base:

$$T_j = T\left(H_{b,j}\right).$$

Finally, heights of the stratiform cloud tops are computed according to $H_{t,j} = H_{b,j} + h_j$. Heights of convective cloud tops are related to the height of the tropopause

$$H_{t,co} = C_{t,co} H_{trop}. \tag{4}$$

Geometric thickness of convective clouds is calculated as $H_{t,co} - H_{b,co}$. In Eq. (4), $C_{t,co}$ is a function of specific humidity (via vertical velocity due to convective stirring w_{conv}, see Eq. 8):

$$C_{t,co} = C_{t,co,1} + C_{t,co,2} \cdot \frac{w_{conv}}{w_{conv,0}} \tag{5}$$

with an additional constraint that $C_{t,co}$ is smaller than the prescribed value $C_{t,co,\,max}$. In Eq. (5), $C_{t,co,1}$ and $C_{t,co,2}$ are constants.

Height of convective clouds base $H_{b,co}$ is related to the planetary boundary layer height

$$H_{b,co} = C_{H,co} H_{PBL}. \tag{6}$$

In addition, effective vertical velocity

$$w_e = w_{ls} + a_{w_E,3} w_{syn} + a_{w_E,4} w_{oro} + a_{w_E,5} w_{conv} \tag{7}$$

is checked to be positive at this level. Otherwise, it is assumed that no convection occurs at a given geographic location. Effective vertical velocity in Eq. (7) is calculated similar to Eq. (36) in Petoukhov et al. (2000), but with coefficients $a_{w_E,3}$ and $a_{w_E,4}$ depending on cloud type. An additional modification with respect to Eq. (36) in Petoukhov et al. (2000) is due to convective stirring: the term $a_{w_E,5} w_{\mathrm{conv}}$ is introduced with

$$w_{\mathrm{conv}} = w_{\mathrm{conv},0} \exp\left(\frac{q_{\mathrm{v}}(0)}{q_{\mathrm{v},0}}\right). \tag{8}$$

Here $q_{\mathrm{v}}(0)$ is near-surface specific humidity, $w_{\mathrm{conv},0} = 0.01\,\mathrm{m\,s^{-1}}$, $q_{\mathrm{v},0} = 0.01\,\mathrm{kg(H_2O)\,kg(air)^{-1}}$. In the scheme, $a_{w_E,5}$ is zeroed for stratiform clouds. Thus, the last term in Eq. (7) is applied only to convective clouds.

Thus calculated heights are associated with the nearest vertical level corresponding to input variables.

2.2 Cloud amount

For stratiform clouds, cloud amounts are calculated similar to Eq. (35) in Petoukhov et al. (2000)

$$c_j = \mathrm{RH}(H_{\mathrm{b},j})^{c_{\mathrm{e},j}} F_{\mathrm{c},w_{\mathrm{e}},j}. \tag{9}$$

Here $\mathrm{RH}(H_{\mathrm{b},j})$ is relative humidity at cloud bases, and

$$F_{\mathrm{c},w_{\mathrm{e}},j} = C_{\mathrm{c,s},1,j} + \frac{1}{2} C_{\mathrm{c,s},2,j} \left(1 + \tanh \frac{w_{\mathrm{e}}\left(H_{\mathrm{b},j}\right)}{C_{\mathrm{c,s},5}}\right). \tag{10}$$

In Eq. (10), $c_{\mathrm{e},j}$, $C_{\mathrm{c,s},1,j}$, $C_{\mathrm{c,s},2,j}$, and $C_{\mathrm{c,s},5}$ are constants.

Convective clouds are allowed to develop only if w_{e} is positive. If this condition is fulfilled, convective cloud amount is computed according to Eq. (38) in Petoukhov et al. (2000):

$$c_{\mathrm{co}} = c_{\mathrm{co},0} \tanh \frac{w_{\mathrm{e}}\left(H_{\mathrm{b,co}}\right)}{C_{\mathrm{c,co},1}} \tanh \frac{q_v(0)}{C_{\mathrm{c,co},2}}. \tag{11}$$

GMDD
6, 3241–3287, 2013

Scheme for cloudiness and precipitation for EMICs

A. V. Eliseev et al.

Title Page
Abstract Introduction
Conclusions References
Tables Figures
◀◀ ▶▶
◀ ▶
Back Close
Full Screen / Esc
Printer-friendly Version
Interactive Discussion

Here $c_{co,0}$, $C_{c,co,1}$, and $C_{c,co,2}$ are constants.

Because stratiform and convective clouds may coexist at a given layer within a given grid cell, it is checked that in every layer $c_{co} + c_j \leq 1$, where c_j is either c_{sl} or c_{sm} or c_{sh}. If this condition is not met, convective cloud amount is reduced to $c_{co} = 1 - c_j$. In other words, if both stratiform and convective clouds coexist in a given grid cell, the former is considered to be favoured.

Total cloud amounts are computed by overlapping clouds at different levels. Convective clouds are always considered as a single column with maximum overlap between individual computational layers. For stratiform clouds, a random overlap between low-, mid-, and upper-level clouds is always used. However, if, say, $H_{t,co} > H_{b,sm}$ then the area covered by cumulus clouds is removed from the latter random overlap for low- and mid-level stratiform clouds. Similar approach, but extended to the upper-level stratiform clouds as well, is used if $H_{t,co} > H_{b,sh}$.

2.3 Cloud water and ice content

For stratiform clouds, cloud water path is calculated after Eq. (2) at page 332 in Mazin and Khrgian (1989):

$$W_j = \alpha_W h_j F_W \tag{12}$$

where

$$F_{W,j} = \exp\left[r_{MK}\left(T_j - T_f\right)\right]/T_j, \tag{13}$$

$T_f = 273.16\,\mathrm{K}$, and α_W is constant. Cloud water content is then distributed vertically, assuming that lateral boundaries of stratiform clouds are vertical and W_j profile is homogeneous within the cloud.

For convective clouds, total cloud water path W_{co} is calculated by integrating the respective vertical profile over the cloud depth

$$W_{co} = \int_{H_{b,co}}^{H_{t,co}} Q_{co}(z)\,dz. \tag{14}$$

Here $Q_{co}(z)$ is volumetric cloud water/ice content which is computed by using Eq. (1) on p. 337 in Mazin and Khrgian (1989):

$$Q_{co}(z) = Q_{co,\,max} \times \left(\frac{\zeta}{\zeta_0}\right)^{m_{MK}} \left(\frac{1-\zeta}{1-\zeta_0}\right)^{n_{MK}} \tag{15}$$

with

$$\zeta = \left(z - H_{b,co}\right) / \left(H_{t,co} - H_{b,co}\right),$$
$$m_{MK} = 2.8,$$
$$n_{MK} = 0.57,$$
$$\zeta_0 = m_{MK} / \left(m_{MK} + n_{MK}\right).$$

In turn, maximum volumetric water/ice content in convective clouds, $Q_{co,\,max}$ is approximated based on Fig. 2 on the same page in Mazin and Khrgian (1989)

$$Q_{co,\,max} = b_{1,MK}\left(H_{t,co} - H_{b,co}\right) + b_{2,MK}\left(T_{co} - 273.16\right) - b_{3,MK} \tag{16}$$

with an additional check that $Q_{co,\,max} \geq 0$.

For all cloud types, ice and droplet clouds are distinguished. The molar fraction of frozen and non-frozen water molecules, f_{ice} and f_{drop} correspondingly, at a given height

GMDD
6, 3241–3287, 2013

z is calculated, respectively, according to Rotstayn (1997):

$$f_{\mathrm{ice}}(z) = \begin{cases} 1, & \text{if} \quad T(z) < T_{\mathrm{m},1} \\ \frac{T_{\mathrm{m},2}-T(z)}{T_{\mathrm{m},2}-T_{\mathrm{m},1}}, & \text{if} \quad T_{\mathrm{m},1} \leq T(z) \leq T_{\mathrm{m},2}, \\ 0, & \text{if} \quad T(z) > T_{\mathrm{m},2}, \end{cases} \tag{17}$$

$$f_{\mathrm{drop}}(z) = 1 - f_{\mathrm{ice}}(z).$$

The values of $T_{\mathrm{m},1}$ and $T_{\mathrm{m},2}$ are assumed to be independent of cloud type.

Total cloud water path (per grid cell) is calculated as follows

$$W_{\mathrm{tot}} = W^{(1)} + W^{(2)} + W^{(3)} \tag{18}$$

with contributions from the grid cell parts covered by one-, two-, and three-layer cloudiness:

$$\begin{aligned}
W^{(1)} &= W^{(1,1)} + W^{(1,2)} + W^{(1,3)} + W^{(\mathrm{co})}, \\
W^{(2)} &= W^{(2,1)} + W^{(2,2)} + W^{(2,3)}, \\
W^{(3)} &= (1 - c_{\mathrm{co}}) c_{\mathrm{sl}} c_{\mathrm{sm}} c_{\mathrm{sh}} (W_{\mathrm{sl}} + W_{\mathrm{sm}} + W_{\mathrm{sh}}), \\
W^{(1,1)} &= (1 - c_{\mathrm{co}}) W_{\mathrm{sl}} c_{\mathrm{sl}} (1 - c_{\mathrm{sm}})(1 - c_{\mathrm{sh}}), \\
W^{(1,2)} &= (1 - c_{\mathrm{co}})(1 - c_{\mathrm{sl}}) W_{\mathrm{sm}} c_{\mathrm{sm}} (1 - c_{\mathrm{sh}}), \\
W^{(1,1)} &= (1 - c_{\mathrm{co}})(1 - c_{\mathrm{sl}})(1 - c_{\mathrm{sm}}) W_{\mathrm{sh}} c_{\mathrm{sh}}, \\
W^{(co)} &= W_{\mathrm{co}} c_{\mathrm{co}} (1 - c_{\mathrm{sl}})(1 - c_{\mathrm{sm}})(1 - c_{\mathrm{sh}}), \\
W^{(2,1)} &= (1 - c_{\mathrm{co}}) W_{\mathrm{sl}} W_{\mathrm{sm}} (c_{\mathrm{sl}} + c_{\mathrm{sm}})(1 - c_{\mathrm{sh}}), \\
W^{(2,2)} &= (1 - c_{\mathrm{co}}) W_{\mathrm{sl}} W_{\mathrm{sh}} (c_{\mathrm{sl}} + c_{\mathrm{sh}})(1 - c_{\mathrm{sm}}), \\
W^{(2,3)} &= (1 - c_{\mathrm{co}}) W_{\mathrm{sm}} W_{\mathrm{sh}} (c_{\mathrm{sm}} + c_{\mathrm{sh}})(1 - c_{\mathrm{sl}}).
\end{aligned}$$

In this equations, W_X and c_X indicate cloud water paths of individual cloud types.

GMDD
6, 3241–3287, 2013

Scheme for cloudiness and precipitation for EMICs

A. V. Eliseev et al.

2.4 Precipitation

Precipitation rate is computed as a sum of large scale (stratiform) and convective precipitation

$$P_{\mathrm{tot}} = P_{\mathrm{ls}} + P_{\mathrm{co}}. \tag{19}$$

Large scale precipitation is calculated by summing the contributions from all stratiform clouds in a given grid cell:

$$P_{\mathrm{ls}} = P_{\mathrm{ls,sl}} + P_{\mathrm{ls,sm}} + P_{\mathrm{ls,sh}},$$

with

$$P_{\mathrm{sl},j} = f_{\mathrm{drop}} P_{\mathrm{ls},j,\mathrm{drop}} + f_{\mathrm{ice}} P_{\mathrm{ls},j,\mathrm{ice}}. \tag{20}$$

In turn,

$$P_{\mathrm{ls},j,k} = \frac{Q_j f_k c_j^{1/2}}{\tau_{j,k}}$$

where j indicates cloud type, k stands for cloud phase (either droplet or ice), Q_j is volumetric water content in clouds, and $\tau_{j,k}$ is life time of cloud type j in phase k.

Convective precipitation is attributed to cumulus clouds. It is calculated by integrating precipitation in vertical direction

$$P_{\mathrm{co}} = \int_{H_{\mathrm{b,co}}}^{H_{\mathrm{t,co}}} p_{\mathrm{co}}(z)\,dz \tag{21}$$

where p_{co} represents contribution to P_{co} from infinitesimally thin vertical layer. The latter is

$$p_{\mathrm{co}} = f_{\mathrm{drop}}(z) p_{\mathrm{co,\,drop}} + f_{\mathrm{ice}}(z) p_{\mathrm{ls,\,ice}}, \tag{22}$$

GMDD
6, 3241–3287, 2013

and contribution from convective clouds in phase k reads

$$p_{\text{co},k} = \frac{Q_{\text{co}} f_k c_{\text{co}}}{\tau_{\text{co},k}}.$$

For all cloud types, life time is calculated similar to that in Petoukhov et al. (2000)

$$\tau_{j,k} = \tau_{0,j,k} \left(1 - a_\tau F_{c,w_\text{e},j}\right) \tag{23}$$

where $j \in \{\text{sl, sm, sh, co}\}$, $k \in \{\text{drop, ice}\}$, and $F_{c,w_\text{e},j}$ is the same as in Eq. (10). In turn,

$$\begin{aligned} \tau_{j,\text{ice}} &= k_{\tau,\text{ice}} \tau_{j,\text{drop}}, && j = \text{sl, sm, sh, co}, \\ \tau_{j,\text{drop}} &= \tau_0, && j = \text{sl, sm, sh}, \\ \tau_{\text{co,drop}} &= \tau_0 / k_{\tau,\text{conv}}, \end{aligned} \tag{24}$$

and τ_0 is a parameter of the scheme.

Note that the partition between ice and liquid cloud particles may be changed during their fall to ground. As a result, it is impractical to use f_ice or f_drop to calculate rain or snowfall rate at the surface. It is assumed to be calculated by the model's land surface scheme based on surface temperature.

3 Calibration

3.1 An approach

At first, the scheme was tuned manually to arrive at the parameter values listed in Table 2. This was done in order to set a reasonable starting point for the automated calibration procedure figured below. Thereafter, this parameter set as well as the simulations with this set are referred to as initial.

GMDD
6, 3241–3287, 2013

In the latter automated calibration, governing parameters of the scheme were sampled by using the Latin Hypercube sampling (McKay et al., 1979; Stein, 1987). We chose only to sample the parameters which are either most uncertain or those which modify the results of calculations with the scheme most strongly. In addition, some parameters are redundant in the scheme (e.g. any change of $w_{\mathrm{conv},0}$ may be compensated by an opposite relative change in the value of $a_{w_{\mathrm{E}},5}$), and for some it is unclear how to prescribe their prior ranges without a loss of consistency with observations (e.g. all parameters adapted from Mazin and Khrgian, 1989, and denoted by subscript MK). The parameters which are varied in the presented simulations are listed in Table 3. This Table also contains the ranges in which these parameters are varied. For all parameters, uniform (non-informative) priors were chosen. Total sample size in parameter space was 5000.

For comparison with observations, only such variables are chosen for which relatively reliable data sets exist. Those variables are total cloud amount c_{tot}, total (vertically integrated over the whole atmospheric depth) cloud water and ice content W_{tot}, and total precipitation rate P_{tot}. In addition, to assess partition between stratiform and convective clouds, a contribution to P_{tot} from large-scale and convective precipitation is assessed as well.

Total score for the scheme is constructed by multiplying the individual skills for cloud amounts S_{c}, cloud water path S_{W}, and precipitation S_{P}

$$S = S_{\mathrm{c}} S_{\mathrm{W}} S_{\mathrm{prec}}. \tag{25}$$

The goal of the optimisation procedure is

$$S \to \max. \tag{26}$$

Skill score for cloud amount is constructed from its globally and annually averaged value, and fields for annual mean, January and July cloud amounts:

$$S_{\mathrm{c}} = S_{\mathrm{c,g}} S_{\mathrm{c,ann}} S_{\mathrm{c,Jan}} S_{\mathrm{c,Jul}}. \tag{27}$$

GMDD
6, 3241–3287, 2013

For globally and annually averaged cloud amount

$$S_{c,g} = \mathcal{N}\left(c_{\text{tot, g,ann,M}}; c_{\text{tot, g,ann,O}}, \sigma_{c_{\text{tot, g,ann,O}}}\right), \quad (28)$$

where is $\mathcal{N}(X; X_m, \sigma_X)$ is a normal distribution function of variable X with mean X_m and standard deviation σ_X. In turn, $c_{\text{tot, g,ann}}$ is the globally and annually averaged total cloud amount. Here and below indices M and O stand for modelled and observed fields, respectively. Skills $S_{\text{c, ann}}$, $S_{\text{c,Jan}}$, and $S_{\text{c,Jul}}$ are computed as in Taylor (2001):

$$S_X = \mathcal{T}_\mathcal{X} \quad (29)$$

where X stands for any of "c,ann", "c,Jan", and "c,Jul" and function

$$\mathcal{T}_\mathcal{X} = \frac{(1 + r_X)^4}{(A_X + 1/A_X)^2}. \quad (30)$$

In Eq. (30) r_X is the coefficient of the spatial correlation between area weighted modelled and observed fields of X, and A_X is the so called relative spatial variation calculated according to

$$A_X = A_{X,\mathrm{M}}/A_{X,\mathrm{O}} \quad (31)$$

where $A^2_{X,\mathrm{M}}$ is the spatial average of $\left(X_\mathrm{M} - X_{\mathrm{M,g}}\right)^2$, and $X_{\mathrm{M,g}}$ is a globally (but not necessarily annually) averaged value of the modelled field X_M. In turn, $A_{X,\mathrm{O}}$ is defined similar to $A_{X,\mathrm{M}}$ but for the observed field.

Skill score for cloud water content is calculated by using an equation similar to Eq. (27):

$$S_\mathrm{W} = S_{\mathrm{W,g}} S_{\mathrm{W,ann}} S_{\mathrm{W,Jan}} S_{\mathrm{W,Jul}}. \quad (32)$$

The meaning of terms in the right hand side of Eq. (32) is analogous to that in Eq. (27). This is only applied for total (vertically integrated) cloud water path W_tot. The procedure to calculate terms in the right hand side of Eq. (32) is again similar to Eqs. (28) and (29).

GMDD
6, 3241–3287, 2013

Precipitation skill score is

$$S_{\rm P} = S_{\rm P,g} S_{\rm P,ann} S_{\rm P,Jan} S_{\rm P,Jul}. \tag{33}$$

Because it is important to distinguish between large scale and convective precipitation, $P_{\rm ls}$ and $P_{\rm conv}$ respectively, individual terms in Eq. (33) are calculated differently from their counterparts in Eqs. (27) and (32). In particular,

$$S_{\rm P,g} = S_{\rm P,tot,g} S_{\rm P,rat,g} \tag{34}$$

where

$$S_{\rm P,tot,g} = \mathcal{N}\left(P_{\rm tot,g,ann,M}; P_{\rm tot,g,ann,O}, \sigma_{P_{\rm tot,g,ann,O}}\right),$$
$$S_{\rm P,rat,g} = \mathcal{N}\left(p_{\rm rat,g,ann,M}; p_{\rm rat,g,ann,O}, \sigma_{p_{\rm rat,g,ann,O}}\right). \tag{35}$$

Here $P_{\rm tot} = P_{\rm ls} + P_{\rm co}$, $p_{\rm rat} = P_{\rm co}/P_{\rm ls}$. Further,

$$S_{\rm P,ann} = S_{\rm P,tot,ann} S_{\rm p,rat,ann} \tag{36}$$

Here

$$S_{\rm P,tot,ann} = \mathcal{T}_{\rm P,tot,ann}, \tag{37}$$
$$S_{\rm p,rat,ann} = \mathcal{T}_{\rm p,rat,ann}, \tag{38}$$

The terms $S_{\rm P,Jan}$ and $S_{\rm P,Jul}$ are calculated by using equations similar to Eqs. (36)–(38) but with respective monthly mean fields in place of annual mean ones.

After that, sampled parameters were subjected to Bayesian averaging (Kass and Raftery, 1995; Hoeting et al., 1999) using total scores S as weights. The ensemble means for all sampled parameters obtained in this way were considered as a calibrated parameter set thereafter in this paper (Table 3), and their standard deviations were considered as a measure of respective allowable range width.

We checked different procedures to obtain this optimal parameter set. In particular, we have tried to zero weights if S's were smaller than the half of their maximum. In this approach, ensemble mean values were basically unchanged but their standard deviations were smaller. In addition, we have tried to manually select a best performing sample and use its parameters as optimal. However, in the latter approach no parameter sample was superior with respect to their Bayesian means.

3.2 Forcing data and observational data sets

The simulations were forced by the monthly mean ERA-40 reanalysis (Simmons and Gibson, 2000) climatology for 1979–2002. Synoptic-scale standard deviations of vertical velocity were calculated by using the 2.5–6 days Murakami filter identically to that used by Petoukhov et al. (2008) and converted to z-coordinates assuming geostrophy. Height of the planetary boundary layer was set equal to 1.5 km, and the value 5.5 km was used for the height of the equivalent barotropic level (Charney and Eliassen, 1949; Hoskins and Karoly, 1981). In the vertical direction, twenty one discrete computational levels were used. The lowermost level was located at the Earth's surface, the next one was at H_{PBL}. Other levels were equally spaced in height up to the tropopause. The latter was diagnosed from the monthly mean ERA-40 data using the conventional definition for thermal tropopause.

For total cloud amounts, the following monthly climatologies were used:

– The International Satellite Cloud Climatology Project (ISCCP), product D2 (Rossow and Duenas, 2004). ISCCP based on 3-hourly radiance data from visible (0.8 µm) and infrared (11 µm) channels measurements with the horizontal resolution 4–7 km from weather geostationary satellites (GEO) (like GMS, GOES East, GOES West, Meteosat, MTSAT, INSAT; see Rossow and Duenas (2004) for more details) and National Oceanic and Atmospheric Administration (NOAA) polar-orbiting (Low Earth Orbit, LEO) satellites. Data are intercalibrated between GEO and LEO satellites. Cloud fraction is derived by using the spectral threshold test and a combination of the spatial and temporal uniformity tests.

- The Clouds and Earth's Radiant Energy System (CERES) (Minnis et al., 2011). This data set was created by simultaneous retrievals of cloud properties and broadband radiative fluxes from the instruments on two LEO Terra and Aqua satellites from Earth Observing System. The data from the Terra satellite with 10:30/22:30 LT equatorial crossing were used. Cloud properties are determined using measurements by the Moderate Resolution Imaging Spectroradiometer (MODIS, see below). MODIS provides measurements in 36 spectral channels with resolution from 0.25 to 1 km. Five of them (with the central wavelengths of 0.65, 1.64, 3.75, 11, and 12 μm) are used in the CERES cloud mask.

- The MODIS Science Team (MODIS-ST) data set (Frey et al., 2008). Instead of the CERES algorithm, 14 of 36 spectral channels of MODIS instruments (with the central wavelengths from 0.66 to 13.94 μm) are used in the MODIS-ST cloud mask algorithm to discriminate cloud pixels from clear sky.

- ERA-40 reanalysis data (Simmons and Gibson, 2000). This data set is affected by imperfections of the forecast model. This is especially true for cloud-related variables belonging to the so-called class "C". However, because our simulations will be forced by the ERA-40 data, it is instructive to compare simulation output with that reanalysis data.

Basically, satellite retrievals reliably detect total cloud amount. However, because of the "satellite view" of cloud layers (upper cloud layers may mask lower ones) mid- and lower-level cloud amounts detection is not straightforward. This is the basic reason why only total cloud amounts rather than cloud amounts in different layers were used for calibration. Another reason is the above-mentioned (see Sect. 2) difference between the definition of the cloud layers in the present scheme and that used in common cloud products. An extensive intercomparison between these data sets was reported by Chernokulsky and Mokhov (2010, 2012). We set $\sigma_{c_{\mathrm{tot,g,ann,O}}}$ to 0.1 which is a typical value for interannual standard deviation of globally averaged total cloud amounts as estimated by using the ISCCP data.

Cloud water path W_{tot} was evaluated against the CERES retrievals (Minnis et al., 2011). In this data set, the cloud water path is computed as function of cloud optical depth and appropriate effective particle size. For $S_{\mathrm{W,g}}$, $\sigma_{c_{W_{\mathrm{tot}},\mathrm{g,ann,O}}}$ is set ad hoc to $0.1 \times c_{W_{\mathrm{tot}},\mathrm{g,ann,O}}$.

Total precipitation is compared with the GPCP-2.2 data set (Global Precipitation Climatology Project, version 2.2, an update from Huffman et al., 2009). Lacking purely empirical data about the subdivision of total precipitation into large-scale and convective ones, we have calibrated the scheme by using the p_{rat} calculated based on ERA-40 data. Note that while global annual precipitation amounts differ by 29 % (Table 4), the spatial pattern of precipitation rate in ERA-40 is close to that in GPCP data. For the GPCP-2.2 data, $\sigma_{P_{\mathrm{tot,g,ann,O}}} = 1.5\,\mathrm{mm\,mo^{-1}}$, $\sigma_{p_{\mathrm{rat,g,ann,O}}} = 0.1$.

We arbitrarily divided these data to training and comparison sets. The training set consists of ISCCP data for cloud amount, CERES data for cloud water path, GPCP data for total precipitation, and ERA-40 data for fraction of large scale precipitation in a total one. All other data were used only for comparison.

For the above-mentioned data, a monthly climatology was constructed for 2001–2006. This period formally differs from that for the forcing data. However, this is not a crucial point for our calibration because the scope of this paper is to determine climatological means.

4 Results of calibration

Basically, the scheme with calibrated parameters agrees better with observations relative to its counterpart with the initial parameter set. This is evident even at the global scale with most marked improvement for cloud water path W_{tot} (Table 4). Slight deterioration is visible for fraction of convective precipitation in total precipitation.

4.1 Cloud amounts

At the global scale, cloud amounts simulated by the scheme with the calibrated parameter set equal 0.59 which is slightly below the observational range 0.60–0.67 (Table 4); more extensive comparison of different empirical data sets leads to the value 0.66 ± 0.02 (Chernokulsky and Mokhov, 2010). The simulated value for the scheme with the calibrated parameters set is very close to that for the version with the initial set of parameters.

When averaged over the Northern Hemisphere, total cloud amounts for each calendar month stay within uncertainty range figured by different empirical data sets (Fig. 1a). This is true even if reanalysis data are discarded and comparison is limited only to satellite data. The agreement is worse for the Southern Hemisphere where total cloud amounts are underestimated throughout the year. For both hemispheres, our scheme correctly simulates minimum (maximum) cloud amount during cold (warm) part of the year. However, the amplitude of the annual cycle for modelled c_{tot} is greater than the satellite-derived one, especially in the Southern Hemisphere.

The scheme broadly reproduces geographical pattern of cloud amounts. Similar to observations, annual mean total cloud amount, c_{tot}, attains maxima in northern and southern mid-latitudes, where c_{tot} is typically between 0.7 and 0.9 (Fig. 2a, b). This is in general agreement with empirically-derived values over oceans (Fig. 2c–f). However, over land our scheme with the initial parameter set overestimates total cloud amount in this latitudes, since satellite-based data show smaller cloud amounts (from 0.5 to 0.7 from ISCCP and MODIS, and even from 0.3 to 0.7 from CERES). This bias is slightly diminished upon calibration. This is accompanied by reduced total cloud amount over mid-latitudinal oceans which worsens the agreement with observations. In the subtropics, the simulated total cloud amounts range from 0.1 to 0.5, which is too small in comparison to observations. Note that too-deep subtropical minima of c_{tot} become shallower upon calibration. The amount of convective clouds over the Indo-Pacific warm

GMDD
6, 3241–3287, 2013

pool and over the Amazonian basin in our scheme (0.7 and larger) generally agrees with observations.

Basic conclusions made for the performance of the scheme for annual mean total cloud amounts may be translated to c_{tot} fields for individual months (Figs. 3 and 4). For all months, the scheme realistically reproduces total cloud amounts over mid-latitudinal oceans, but overestimates c_{tot} over land at the same latitudes. That overestimate is more marked in winter than in summer, which is consistent with the overestimated amplitude of the annual cycle of c_{tot}. Subtropical minima are too deep throughout the year. However, the scheme correctly places abundant convective clouds near the equator in the winter hemisphere.

Comparison of the simulated cloud amounts in different layers with observations is not straightforward. The first reason for that is due to difference in classification of cloud layers between the proposed scheme, on one hand, and common satellite cloud products, on the other. In our scheme, clouds belong to a particular layer depending on the height of cloud bases (see Sect. 2.2). As a result, convective clouds always belong to the lower layer in our scheme. This is in contrast with satellite retrievals which classify clouds based on their tops. There, convective clouds may be classified either to low- or to mid- or to upper-level clouds depending on vertical extent of convective cloud ensemble. Another reason leading to difficulties in comparison of cloud amounts in individual layers is due to the above-mentioned "satellite view" of cloud layers in common cloud satellite products (see Sect. 3.2).

However, some comparison may be performed with the results reported by Mace et al. (2009) who used the same classification scheme as we do for the merged lidar and radar observations from CALIPSO and CloudSat satellites. This comparison is flawed because Mace et al. (2009) uses only one year of measurements (from July 2006 to June 2007), but is still instructive. For reader's convenience, Fig. 5 is redrawn in the Supplement to the present paper (Fig. S1) in a fashion compatible with relevant Figures from Mace et al. (2009). In turn, the latter figures are reproduced in Fig. S2 of Supplement with permission of Wiley and Sons Inc.

GMDD
6, 3241–3287, 2013

In particular, our annual mean low-level cloud amount $c_l = c_{sl} + c_{co}$ may be compared to their Fig. 10a. Our scheme with the initial parameter set simulates c_l between 0.6 and 0.7 over the mid-latitudes and in the areas of tropical convection, and from 0.1 to 0.5 in the subtropics (Fig. 5a). The largest c_l (above 0.7) is simulated over the Antarctic. Upon calibration, c_l in the northern and southern mid-latitudes is from 0.4 to 0.6, and over the Antarctic it is increased to values 0.8 and larger. (Fig. 5b). In the middle latitudes, the calibration improves the agreement with the retrievals by Mace et al. (2009). In the subtropics, c_l is increased somewhat which again improves the agreement. Maxima of c_l over the Indo-Pacific warm pool and over Amazonia become broader which deteriorates our simulations.

One major weak point of the present scheme is the lack of stratocumulus (Sc) decks over the eastern parts of the oceans. Annual mean stratocumulus cloud amount in these regions amounts up to 0.6 (Wood, 2012) and yields about 80–90 % of all low-level cloud fraction here. Our scheme produces low-level cloud fractions in these regions smaller than 0.2, which underestimate markedly the observed one. Note, however, that ERA-40 data underestimate the satellite-derived cloud amount in these regions as well.

Mid-level cloud amounts $c_m \equiv c_{sm}$ may be compared with Fig. 11 from Mace et al. (2009). In the version with the initial parameter set, mid-level cloud amounts range from 0.3 to 0.5 in mid-latitudes and the convective regions in the tropics (Fig. 5c). In other tropical and subtropical regions, c_m is below 0.2 everywhere. Upon calibration, everywhere in the tropics and subtropics $c_m < 0.1$, and in higher latitudes c_m is between 0.1 and 0.2 (Fig. 5d). This drastically improves agreement with the hydrometeor fractions with bases from 3 km to 6 km reported in Fig. 11 of Mace et al. (2009).

The modelled upper-level cloud amounts $c_h \equiv c_{sh}$ markedly increase during calibration. In the version with the initial parameter set, annual mean c_h is below 0.2 everywhere over the globe (Fig. 5e). Upon calibration, c_h increases to 0.2–0.4 in the middle and high latitudes of the Northern and Southern Hemispheres as well as over convective regions in the tropics (Fig. 5f). As compared to Fig. 12a from Mace et al. (2009), our calibration substantially improves the scheme's performance. In particular,

GMDD
6, 3241–3287, 2013

extra-tropical upper-level cloud amounts become broadly realistic, while there is an underestimation of c_h in the areas of tropical convection by a factor of two.

4.2 Cloud water path

Cloud water path (per model grid cell) W_{tot} is markedly increased during calibration. In the initial version, globally and annually averaged W_{tot} equals to 66 g(H_2O) m^{-2}, which is about a half of respective value derived from CERES, 125 g(H_2O) m^{-2} (Table 4). After calibration, modelled W_{tot} increases to 82 g(H_2O) m^{-2}, which is again too small in comparison to observations but the agreement is better.

The modelled cloud water path averaged over the Northern and Southern Hemispheres show maxima in summer (Fig. 6).

Calibration slightly decreases W_{tot} in the extra-tropics throughout the year and markedly increases it in the tropics. Annual mean cloud water path in both versions of the scheme is from 20 g(H_2O) m^{-2} to 80 g(H_2O) m^{-2} (Fig. 7a). Over land it broadly agrees with the CERES data. Over oceans, it is an underestimate (Fig. 7c). In the tropics, calibration increases annual mean W_{tot} by 20–50 %. As a result, the calibrated values of W_{tot} in the tropics agree better with the CERES data than the initial ones. In addition, W_{tot} is too small in comparison to the CERES data. However, in these regions the CERES suffer from large uncertainty (Minnis et al., 2011).

In winter, cloud water path is severely underestimated especially over land (Figs. 8 and 9). While in the high latitudes one has to bear in mind large uncertainty of the CERES retrievals, in the middle latitudes an underestimate is clear. In summer, mid-latitudinal cloud water path is somewhat small in comparison to the CERES data, but reasonable as a whole. In contrast, in the tropics, W_{tot} is somewhat too high but the latter bias is markedly smaller than that in the middle latitudes in winter.

The largest contribution to W_{tot} comes from low-level stratiform clouds during all seasons, and from mid-level stratiform clouds during the warm part of the year (not shown). In the tropics, the contribution from convective clouds is also valuable.

GMDD
6, 3241–3287, 2013

4.3 Precipitation

Annual global precipitation changes insignificantly during calibration. In the version with the initial parameter set it equals to 101 $cm\,yr^{-1}$, and in the calibrated version it is 100 $cm\,yr^{-1}$. Both values are within the range set by the GPCP data 88 $cm\,yr^{-1}$ and by the ERA-40 113 $cm\,yr^{-1}$ (Table 4). The fraction of large scale precipitation in the initial version is 0.48, which is an underestimate relative to the ERA-40 data (0.53). It becomes even smaller (0.45) after calibration (Table 4).

For monthly precipitation averaged over the Northern and Southern Hemispheres, both initial and calibrated versions reasonably agree with empirical climatologies (Fig. 10). Basically, calibration enhances precipitation in the tropics and in the monsoon area and suppresses elsewhere. In the calibrated version, monthly precipitation in the Northern (Southern) Hemisphere changes from 7 $cm\,mo^{-1}$ (6 $cm\,mo^{-1}$) in winter to 11 $cm\,mo^{-1}$ (14 $cm\,mo^{-1}$) in summer.

Upon calibration, annual precipitation slightly decreases in the middle latitudes and in the monsoon-affected region and markedly increases in the tropics (Fig. 11a, b). In the calibrated version, precipitation P_{tot} is from 90 $cm\,yr^{-1}$ to 180 $cm\,yr^{-1}$ in the middle latitudes. This is a decrease by about one fourth from the initial version. In turn, in the moist tropics and subtropics, the calibrated precipitation is from 180 $cm\,yr^{-1}$ to 300 $cm\,yr^{-1}$ which is a respective increase by a factor 1.5 (up to 2.5 in the region affected by the East Asian monsoon). In dry subtropics, precipitation is not changed markedly during calibration, being below 60 $cm\,yr^{-1}$. In most regions, the calibrated annual precipitation values agree much better with the GPCP and ERA-40 climatologies than the initial ones.

One observes the marked decrease in the calibrated values relative to initial ones in the middle latitudes of the winter hemisphere (Figs. 12a, b and 13a, b). In January, precipitation over Eastern Eurasia is diminished from 2–5 $cm\,mo^{-1}$ in the initial version to 1–3 $cm\,mo^{-1}$. The latter much better agrees with the empirical data in comparison to the former one (Fig. 12c, d). Over northern mid-latitudinal oceans, during calibration

GMDD
6, 3241–3287, 2013

winter precipitation is decreased by a factor of two or three. In the calibrated version it is from $4\,\mathrm{cm\,mo^{-1}}$ to $16\,\mathrm{cm\,mo^{-1}}$ over northern mid-latitudinal oceans in January, and from $6\,\mathrm{cm\,mo^{-1}}$ to $20\,\mathrm{cm\,mo^{-1}}$ over southern-mid-latitudinal oceans in July. Both ranges are in agreement with empirical data (Figs. 12c, d and 13c, d).

Another important change during calibration is a marked increase of precipitation in the tropical convective regions throughout the year as well as in the monsoon regions in Asia. In the convective regions, precipitation is enhanced by a factor 1.5–2. Even more pronounced enhancement occurs in the monsoon-affected region in south-eastern Asia where summer precipitation is increased by a factor 2–2.5. All these changes substantially improve agreement between modelled and empirically-derived precipitation.

5 Conclusions

This paper presents a scheme for calculation of the characteristics of multi-layer cloudiness and associated precipitation designed for climate models of intermediate complexity (EMICs). In contrast to the respective schemes previously used in the models of this class, the scheme considers three-layer stratiform cloudiness and single column convective clouds. It distinguishes between ice and droplet clouds as well. All main cloudiness characteristics (cloud amount, cloud water path) are calculated interactively. Precipitation is calculated by using cloud life time, which depends on cloud type and phase as well as on statistics of synoptic and convective disturbances.

A novel approach for tuning this scheme was used. This approach was based on sampling of major governing parameters of the scheme. The corresponding cost function was constructed based on total cloud amount, cloud water path, and precipitation, taking into account global mean values and annual mean, January, and July spatial distributions for these variables. Bayesian averaging was used to calculate the optimal parameters set.

After calibration, the scheme realistically reproduces main characteristics of cloudiness and precipitation. The simulated globally and annually averaged total cloud amount is 0.59, and the simulated globally averaged annual precipitation is 109 $\mathrm{cm\,yr^{-1}}$. Both values agree with empirically-derived values.

The scheme agrees with observations for total cloud amounts over mid-latitudinal oceans, but overestimates c_{tot} over land at the same latitudes. The latter overestimate is more marked in winter than in summer. Subtropical minima are too deep throughout the year. The scheme correctly places abundant convective clouds near the equator in the winter hemisphere, while it underestimates upper-level cloud amount in the regions with strong convection.

Cloud water path is severely overestimated by the scheme. In particular, major storm tracks contain too much water. However, cloud water path of tropical convective clouds is reproduced reasonably.

Upon calibration, the total precipitation as well as fraction of large scale precipitation in total precipitation agree reasonably with empirical data.

Note that our calibration is not a simple "fitting exercise". In particular, cloud amounts at different layers were not trained explicitly during calibration. Nevertheless, they agree with available (rather limited) empirical data. This poses some confidence on physical basis of our scheme.

However, regional and seasonal biases still present in the calibrated version show that there is a room for improvement of the scheme. One line of improvement may be implementation of stratiform cloud amounts originated from convective anvils in the upper troposphere in presence of strong winds (Mazin and Khrgian, 1989; Houze, 1994). This may ameliorate too small upper-level cloud amounts in the tropical convective regions in the current version of the scheme. Another major improvement should be an implementation of stratocumulus decks representation, which should improve cloudiness over the eastern parts of the oceans. This implementation has to take into account inversion layers trapping convection and limiting vertical development of convective clouds (Wood, 2012). In addition, this version of the scheme lacks

GMDD
6, 3241–3287, 2013

aerosol–cloudinteraction (Twomey, 1974; Albrecht, 1989; Hobbs, 1993; Lohmann and Feichter, 2005). We note that one approach to include the latter in climate models of intermediate complexity was developed by Bauer et al. (2008). An updated version of their scheme is planned to be implemented in our scheme in the future.

Supplementary material related to this article is available online at: http://www.geosci-model-dev-discuss.net/6/3241/2013/gmdd-6-3241-2013-supplement.pdf.

Acknowledgements. This work has been supported by the President of Russia grants 5467.2012.5 and 3259.2012.5, by the Russian Foundation for Basic Research, and by the Programs of the Russian Ministry for Science and Education (contract 14.740.11.1043 and agreement 8617), and the Russian Academy of Sciences (programs of the Presidium RAS, programs by the Department of Earth Sciences RAS, and contract 74-OK/1-4).

References

Albrecht, B.: Aerosols, cloud microphysics, and fractional cloudiness, Science, 245, 1227–1230, 1989. 3265

Bauer, E., Petoukhov, V., Ganopolski, A., and Eliseev, A.: Climatic response to anthropogenic sulphate aerosols versus well-mixed greenhouse gases from 1850 to 2000 AD in CLIMBER-2, Tellus, 60B, , 82–97, doi:10.1111/j.1600-0889.2007.00318.x, 2008. 3265

Bony, S., Colman, R., Kattsov, V., Allan, R., Bretherton, C., J.-L., D., Hall, A., Hallegatte, S., Holland, M., Ingram, W., Randall, D., Soden, B., Tselioudis, G., and Webb, M.: How well do we understand and evaluate climate change feedback processes?, J. Climate, 19, 3445–3482, doi:10.1175/JCLI3819.1, 2006. 3242

Cesana, G. and Chepfer, H.: How well do climate models simulate cloud vertical structure? A comparison between CALIPSO-GOCCP satellite observations and CMIP5 models, Geophys. Res. Lett., 39, L20803, doi:10.1029/2012GL053153, 2012. 3242

Charlson, R., Schwartz, S., Hales, J., Cess, R., Coackley, J., Hansen, J., and Hofmann, D.: Climate forcing by anthropogenic aerosols, Science, 255, 423–430, doi:10.1126/science.255.5043.423, 1992. 3243

Charney, J. and Eliassen, A.: A numerical method for predicting the perturbations of the middle latitude westerlies, Tellus, 1, 38–54, doi:10.1111/j.2153-3490.1949.tb01258.x, 1949. 3255

Chernokulsky, A. and Mokhov, I.: Intercomparison of global and zonal cloudiness characteristics from different satellite and ground based data, Issledovaniye Zempli iz Kosmosa, 12–29, 2010 (in Russian). 3257, 3258

Chernokulsky, A. and Mokhov, I.: Climatology of total cloudiness in the Arctic: an intercomparison of observations and reanalyses, Advances in Meteorology, 2012, 542093, doi:10.1155/2012/542093, 2012. 3257

Claussen, M., Mysak, L., Weaver, A., Crucifix, M., Fichefet, T., Loutre, M.-F., Weber, S., Alcamo, J., Alexeev, V., Berger, A., Calov, R., Ganopolski, A., Goosse, H., Lohmann, G., Lunkeit, F., Mokhov, I., Petoukhov, V., Stone, P., and Wang, Z.: Earth system models of intermediate complexity: closing the gap in the spectrum of climate system models, Clim. Dynam., 18, 579–586, doi:10.1007/s00382-001-0200-1, 2002. 3243

Coumou, D., Petoukhov, V., and Eliseev, A.: Three-dimensional parameterizations of the synoptic scale kinetic energy and momentum flux in the Earth's atmosphere, Nonlinear. Proc. Geoph., 18, 807–827, doi:10.5194/npg-18-807-2011, 2011. 3243

Dufresne, J.-L. and Bony, S.: An assessment of the primary sources of spread of global warming estimates from coupled atmosphere-ocean models, J. Climate, 21, 5135–5144, doi:10.1175/2008JCLI2239.1, 2008. 3242

Eby, M., Weaver, A. J., Alexander, K., Zickfeld, K., Abe-Ouchi, A., Cimatoribus, A. A., Crespin, E., Drijfhout, S. S., Edwards, N. R., Eliseev, A. V., Feulner, G., Fichefet, T., Forest, C. E., Goosse, H., Holden, P. B., Joos, F., Kawamiya, M., Kicklighter, D., Kienert, H., Matsumoto, K., Mokhov, I. I., Monier, E., Olsen, S. M., Pedersen, J. O. P., Perrette, M., Philippon-Berthier, G., Ridgwell, A., Schlosser, A., Schneider von Deimling, T., Shaffer, G., Smith, R. S., Spahni, R., Sokolov, A. P., Steinacher, M., Tachiiri, K., Tokos, K., Yoshimori, M., Zeng, N., and Zhao, F.: Historical and idealized climate model experiments: an EMIC intercomparison, Clim. Past Discuss., 8, 4121–4181, doi:10.5194/cpd-8-4121-2012, 2012. 3243

Eliseev, A., Mokhov, I., and Muryshev, K.: Estimates of climate changes in the 20th–21st centuries based on the version of the IAP RAS climate model including the model of general

ocean circulation, Russ. Meteorol. Hydrol., 36, 73–81, doi:10.3103/S1068373911020014, 2011. 3243
Frey, R., Ackerman, S., Liu, Y., Strabala, K., Zhang, H., Key, J., and Wang, X.: Cloud detection with MODIS. Part 1: Improvements in the MODIS cloud mask for collection 5, J. Atmos. Ocean. Tech., 25, 1057–1072, doi:10.1175/2008JTECHA1052.1, 2008. 3256
Ganopolski, A., Petoukhov, V., Rahmstorf, S., Brovkin, V., Claussen, M., Eliseev, A., and Kubatzki, C.: CLIMBER-2: a climate system model of intermediate complexity. Part 2: Model sensitivity, Clim. Dynam., 17, 735–751, doi:10.1007/s003820000144, 2001. 3243
Hobbs, P. (Ed.): Aerosol-Cloud-Climate Interactions, Academic Press, London, San Diego, 1993. 3265
Hoeting, J., Madigan, D., Raftery, A., and Volinsky, C.: Bayesian model averaging: a tutorial, Stat. Sci., 14, 382–401, 1999. 3254
Hoskins, B. and Karoly, D.: The steady linear response of a spherical atmosphere to thermal and orographic forcing, J. Atmos. Sci., 38, 1179–1196, doi:10.1175/1520-0469(1981)038<1179:TSLROA>2.0.CO;2, 1981. 3255
Houze, R.: Cloud Dynamics, Academic Press, San Diego, 1994. 3264
Huffman, G., Adler, R., Bolvin, D., and Gu, G.: Improving the global precipitation record: GPCP Version 2.1, Geophys. Res. Lett., 36, L17808, doi:10.1029/2009GL040000, 2009. 3257
Kass, R. and Raftery, A.: Bayes factors, J. Am. Stat. Assoc., 90, 773–795, 1995. 3254
Liou, K.: An Introduction to Atmospheric Radiation, Academic Press, San Diego, 2002. 3243
Lohmann, U. and Feichter, J.: Global indirect aerosol effects: a review, Atmos. Chem. Phys., 5, 715–737, doi:10.5194/acp-5-715-2005, 2005. 3265
Mace, G., Zhang, Q., Vaughan, M., Marchand, R., Stephens, G., Trepte, C., and Winker, D.: A description of hydrometeor layer occurrence statistics derived from the first year of merged Cloudsat and CALIPSO data, J. Geophys. Res., 114, D00A26, doi:10.1029/2007JD009755, 2009. 3259, 3260
Mazin, I. and Khrgian, A.: Handbook of Clouds and Cloudy Atmosphere, Gidrometeoizdat, Leningrad, 1989 (in Russian). 3244, 3247, 3248, 3252, 3264
McKay, M., Beckman, R., and Conover, W.: A comparison of three methods for selecting values of input variables in the analysis of output from a computer code, Technometrics, 21, 239–245, 1979. 3252
Minnis, P., Sun-Mack, S., Young, D., Heck, P., Garber, D., Chen, Y., Spangenberg, D., Arduini, R., Trepte, Q., Smith, W., Ayers, J., Gibson, S., Miller, W., Chakrapani, V., Takano, Y.,

Liou, K.-N., Xie, Y., and Yang, P.: CERES Edition-2 cloud property retrievals using TRMM VIRS and Terra and Aqua MODIS data, Part 1: Algorithms, IEEE T. Geosci. Remote, 49, 4374–4400, 2011. 3256, 3257, 3261

Mokhov, I. and Eliseev, A.: Modeling of global climate variations in the 20th–23rd centuries with new RCP scenarios of anthropogenic forcing, Doklady Earth Sci., 443, 532–536, doi:10.1134/S1028334X12040228, 2012. 3243

Montoya, M., Griesel, A., Levermann, A., Mignot, J., Hofmann, M., Ganopolski, A., and Rahmstorf, S.: The earth system model of intermediate complexity CLIMBER-3α. Part I: Description and performance for present-day conditions, Clim. Dynam., 25, 237–263, doi:10.1007/s00382-005-0044-1, 2005. 3243

Petoukhov, V., Mokhov, I., Eliseev, A., and Semenov, V.: The IAP RAS Global Climate Model, Dialogue-MSU, Moscow, 1998. 3244

Petoukhov, V., Ganopolski, A., Brovkin, V., Claussen, M., Eliseev, A., Kubatzki, K., and Rahmstorf, S.: CLIMBER-2: a climate system model of intermediate complexity. Part 1: model description and performance for present climate, Clim. Dynam., 16, 1–17, doi:10.1007/PL00007919, 2000. 3243, 3244, 3245, 3246, 3251

Petoukhov, V., Ganopolski, A., and Claussen, M.: POTSDAM – a Set of Atmosphere Statistical-Dynamical Models: Theoretical Background, Tech. Rep. PIK Rep. 81, Potsdam-Institut für Klimafolgendforschung, Potsdam, 2003. 3244

Petoukhov, V., Claussen, M., Berger, A., Crucifix, M., Eby, M., Eliseev, A., Fichefet, T., Ganopolski, A., Goosse, H., Kamenkovich, I., Mokhov, I., Montoya, M., Mysak, L., Sokolov, A., Stone, P., Wang, Z., and Weaver, A.: EMIC intercomparison project (EMIP-CO_2): comparative analysis of EMIC simulations of current climate and equilibrium and transient reponses to atmospheric CO_2 doubling, Clim. Dynam., 25, 363–385, doi:10.1007/s00382-005-0042-3, 2005. 3243

Petoukhov, V., Eliseev, A., Klein, R., and Oesterle, H.: On statistics of the free-troposphere synoptic component: an evaluation of skewnesses and mixed third-order moments contribution to the synoptic-scale dynamics and fluxes of heat and humidity, Tellus, 60A, 11–31, doi:10.1111/j.1600-0870.2007.00276.x, 2008. 3255

Rossow, W. and Duenas, E.: The International Satellite Cloud Climatology Project (ISCCP) web site: an online resource for research, B. Am. Metereol. Soc., 85, 167–172, doi:10.1175/BAMS-85-2-167, 2004. 3255

Rotstayn, L.: A physically based scheme for the treatment of stratiform clouds and precipitation in large-scale models. I: description and evaluation of the microphysical processes, Q. J. Roy. Meteor. Soc., 123, 1227–1282, doi:10.1002/qj.49712354106, 1997. 3249

Simmons, A. and Gibson, J.: The ERA-40 Project Plan, ERA-40 Project Rep. Ser. 1, European Center for Medium-Range Weather Forecasting, Reading, 2000. 3255, 3256

Soden, B. and Vecchi, G.: The vertical distribution of cloud feedback in coupled ocean-atmosphere models, Geophys. Res. Lett., 38, L12704, doi:10.1029/2011GL047632, 2011. 3242

Solomon, S., Qin, D., Manning, M., Marquis, M., Averyt, K., Tignor, M., LeRoy Miller, H., and Chen, Z. (Eds.): Climate Change 2007: The Physical Science Basis, Cambridge University Press, Cambridge, New York, 2007. 3242, 3243

Stein, M.: Large sample properties of simulations using latin hypercube sampling, Technometrics, 29, 141–150, doi:10.2307/1269769, 1987. 3252

Stephens, G.: Radiation profiles in extended water clouds. I: Theory, J. Atmos. Sci., 35, 2111–2122, doi:10.1175/1520-0469(1978)035<2111:RPIEWC>2.0.CO;2, 1978. 3243

Stephens, G.: Cloud feedbacks in the climate system: a critical review, J. Climate, 18, 237–273, doi:10.1175/JCLI-3243.1, 2005. 3242

Taylor, K.: Summarizing multiple aspects of model performance in a single diagram, J. Geophys. Res., 106, 7183–7192, doi:10.1029/2000JD900719, 2001. 3253

Tian, L. and Curry, J.: Cloud overlap statistics, J. Geophys. Res., 94, 9925–9935, doi:10.1029/JD094iD07p09925, 1989. 3244

Twomey, S.: Pollution and the planetary albedo, Atmos. Environ., 8, 1251–1256, 1974. 3265

Williams, K. and Tselioudis, G.: GCM intercomparison of global cloud regimes: present-day evaluation and climate change response, Clim. Dynam., 29, 231–250, doi:10.1007/s00382-007-0232-2, 2007. 3242

Wood, R.: Stratocumulus clouds, Mon. Weather Rev., 140, 2373–2423, doi:10.1175/MWR-D-11-00121.1, 2012. 3260, 3264

Zhang, M., Lin, W., Klein, S., Bacmeister, J., Bony, S., Cederwall, R., Del Genio, A., Hack, J., Loeb, N., Lohmann, U., Minnis, P., Musat, I., Pincus, R., Stier, P., Suarez, M., Webb, M., Wu, J., Xie, S., Yao, M.-S., and Zhang, J.: Comparing clouds and their seasonal variations in 10 atmospheric general circulation models with satellite measurements, J. Geophys. Res., 110, D15S02, doi:10.1029/2004JD005021, 2005. 3242

Zickfeld, K., Eby, M., Alexander, K., Weaver, A., Crespin, E., Fichefet, T., Goosse, H., Philippon-Berthier, G., Edwards, N., Holden, P., Eliseev, A., Mokhov, I., Feulner, G., Kienert, H., Perrette, M., Schneider von Deimling, T., Forest, C., Friedlingstein, P., Joos, F., Spahni, R., Steinacher, M., Kawamiya, M., Tachiiri, K., Kicklighter, D., Monier, E., Schlosser, A., Sokolov, A., Matsumoto, K., Tokos, K., Olsen, S., Pedersen, J., Ridgwell, A., Shaffer, G., Yoshimori, M., Zeng, N., and Zhao, F.: Long-term climate change commitment and reversibility: an EMIC intercomparison, J. Climate, doi:10.1175/JCLI-D-12-00584.1, accepted, 2013. 3243

GMDD

6, 3241–3287, 2013

Scheme for cloudiness and precipitation for EMICs

A. V. Eliseev et al.

Title Page
Abstract Introduction
Conclusions References
Tables Figures
Back Close
Full Screen / Esc
Printer-friendly Version
Interactive Discussion

Table 1. List of symbols used throughout the paper. Long dash in the first column indicates that corresponding variable is non-dimensional. Variable modifiers: j indicates cloud type (= sl, sm, sh, conv), k stands for cloud phase (= drop, ice).

variable and units	description
$H_{b,j}$ [m]	height of cloud base
$H_{t,j}$ [m]	height of cloud top
H_{EBL} [m]	height of the equivalent barotropic level
H_{PBL} [m]	height of the top of the planetary boundary layer
H_{trop} [m]	height of the tropopause
h_j [m]	cloud thickness
c_j [–]	cloud amount
c_{tot} [–]	total cloud amount
P_{conv} [kg(H$_2$O) m^{-2} s^{-1}]	convective precipitation
P_{ls} [kg(H$_2$O) m^{-2} s^{-1}]	large scale precipitation
P_{tot} [kg(H$_2$O) m^{-2} s^{-1}]	total precipitation
q [kg(H$_2$O) kg(air)$^{-1}$]	specific humidity
T [K]	temperature
W_j [kg(H$_2$O) m^{-3}]	cloud water/ice content per unit volume
W_{tot} [kg(H$_2$O) m^{-2}]	vertically integrated cloud water/ice content per unit area
w_{eff} [m s^{-1}]	effective vertical velocity (see Eq. 7)
w_{ls} [m s^{-1}]	large-scale vertical velocity
w_{syn} [m s^{-1}]	synoptic-scale standard deviation of vertical velocity

GMDD
6, 3241–3287, 2013

Table 2. List of the standard values of the governing parameters of the scheme. Long dash in the first column indicates that corresponding variable is non-dimensional, and in the last column it shows that specific parameter is not applied to cumulus clouds.

variable and units	value
$C_{H,\mathrm{sl}}$ [–]	1.01
$C_{H,\mathrm{sm}}$ [–]	0.8
$C_{H,\mathrm{sh}}$ [–]	0.8
$C_{\mathrm{H,co}}$ [–]	1
$C_{\mathrm{c,s,5}}$ $[\mathrm{m\,s^{-1}}]$	1.0×10^{-2}
$w_{\mathrm{conv,0}}$ $[\mathrm{m\,s^{-1}}]$	1.0×10^{-2}
$q_{\mathrm{v,0}}$ $[\mathrm{kg(H_2O)\,kg(air)^{-1}}]$	1.0×10^{-2}
$c_{\mathrm{co,0}}$ [–]	0.8
$C_{\mathrm{c,co,1}}$ $[\mathrm{m\,s^{-1}}]$	1.0×10^{-3}
$C_{\mathrm{c,co,2}}$ $[\mathrm{kg(H_2O)\,kg(air)^{-1}}]$	3.0×10^{-2}
c_{h} [–]	0.5
$C_{\mathrm{h,s},k}$ $[\mathrm{K^{-1}}]$	3×10^{-2}
$C_{\mathrm{h,s,m}}$ [K]	278
$C_{\mathrm{t,co,1}}$ [–]	0.5
$C_{\mathrm{t,co,2}}$ [–]	0.2
$C_{\mathrm{t,co,max}}$ [–]	0.9
α_{W} $[\mathrm{kg\,K\,m^{-3}}]$	5.25×10^{-2}
r_{MK} $[\mathrm{K^{-1}}]$	4.3×10^{-2}
m_{MK} [–]	2.8
n_{MK} [–]	0.57
$b_{1,\mathrm{MK}}$ $[\mathrm{g\,m^{-4}}]$	1.2957×10^{-5}
$b_{2,\mathrm{MK}}$ $[\mathrm{g\,m^{-3}\,{}^{\circ}C^{-1}}]$	5.895×10^{-4}
$b_{3,\mathrm{MK}}$ $[\mathrm{g\,m^{-3}}]$	0.7848×10^{-2}
$T_{\mathrm{m,1}}$ [K]	260.0
$T_{\mathrm{m,2}}$ [K]	273.2
τ_0 [s]	0.7×10^{3}
$k_{\tau,\mathrm{conv}}$ [–]	10
$k_{\tau,\mathrm{ice}}$ [–]	2

	SL	SM	SH	CO
$a_{w_E,3}$ [–]	5.0	2.0	2.0	0.5
$a_{w_E,4}$ [–]	0.3	0.3	0.3	0.1
$a_{w_E,5}$ [–]	0.0	0.0	0.0	0.5
c_{e} [–]	1.5	1.5	1.5	–
$C_{\mathrm{c,s,1}}$ [–]	0.1	0.0	0.0	–
$C_{\mathrm{c,s,2}}$ [–]	0.8	0.9	0.3	–
h_0 [m]	4×10^{2}	4×10^{2}	3×10^{3}	–
a_τ [–]	0.990	0.990	0.990	0.998

Table 3. List of the perturbed parameters of the scheme together with their priory ranges. Long dash in the first column indicates that corresponding variable is non-dimensional. The symbols “SL”, “SM”, “SH”, and “CO” indicate particular cloud types according to classification used in the scheme. In the last column, Bayesian mean and standard deviation are shown.

variable and units		sampled range	posterior value
$C_{h,sm}$ [–]		0.6–1.0	0.846 ± 0.012
$C_{t,co,1}$ [–]		0.4–0.6	0.483 ± 0.045
$C_{t,co,2}$ [–]		0.08–0.25	0.167 ± 0.028
$C_{t,co,max}$ [–]		0.85–1.0	0.935 ± 0.014
$C_{co,0}$ [–]		0.70–0.90	0.838 ± 0.008
$C_{c,co,1}$ [$m\,s^{-1}$]		$(0.8 - 1.2) \times 10^{-3}$	$(0.884 \pm 0.084) \times 10^{-3}$
$C_{c,co,2}$ [$kg(H_2O)\,kg(air)^{-1}$]		$(2.0 - 5.0) \times 10^{-2}$	$(2.67 \pm 0.21) \times 10^{-2}$
α_W [$kg\,K\,m^{-3}$]		$(3.0 - 7.0) \times 10^{-2}$	$(5.49 \pm 0.17) \times 10^{-2}$
$T_{m,1}$ [K]		250–265	250.5 ± 0.2
τ_0 [s]		$(0.3 - 1.2) \times 10^3$	$(0.81 \pm 0.07) \times 10^3$
$k_{\tau,conv}$ [–]		4.0–13.0	10.7 ± 0.8
$k_{\tau,ice}$ [–]		1.4–2.6	2.06 ± 0.24
h_0 [m]	SL	$(2 - 6) \times 10^2$	$(3.93 \pm 0.35) \times 10^2$
	SM	$(2 - 6) \times 10^2$	$(2.7 \pm 1.1) \times 10^2$
	SH	$(0.5 - 1.2) \times 10^3$	$(0.84 \pm 0.11) \times 10^3$
$a_{w_E,3}$ [–]	SL	3–7	6.72 ± 0.31
	SM, SH	1–3	2.53 ± 0.33
	CO	0.3–0.8	0.549 ± 0.085
$a_{w_E,4}$ [–]	SL, SM, SH	0.2–0.4	0.373 ± 0.059
	CO	0–0.2	0.185 ± 0.028
$a_{w_E,5}$ [–]	CO	0.3–0.7	0.651 ± 0.019
$C_{c,s,1}$ [–]	SL	0–0.2	0.183 ± 0.031
	SM, SH	0–0.1	0.0121 ± 0.0069
$C_{c,s,2}$ [–]	SL	0.1–1.0	0.817 ± 0.031
	SM	0.1–1.0	0.212 ± 0.056
	SH	0.1–1.0	0.481 ± 0.069

GMDD
6, 3241–3287, 2013

Table 4. Globally and annually averaged values as calculated by the proposed scheme with two parameter sets in comparison with the available observational data.

variable	initial	calibrated	observational datasets
c_{tot} [–]	0.59	0.59	0.62 (ISCCP) 0.67 (MODIS) 0.60 (CERES) 0.64 (ERA-40)
W_{tot} [g(H$_2$O) m^{-2}]	66	82	125 (CERES)
P_{tot} [cm yr^{-1}]	101	100	88 (GPCP) 113 (ERA-40)
P_{ls}/P_{tot} [–]	0.48	0.45	0.53 (ERA-40)

GMDD
6, 3241–3287, 2013

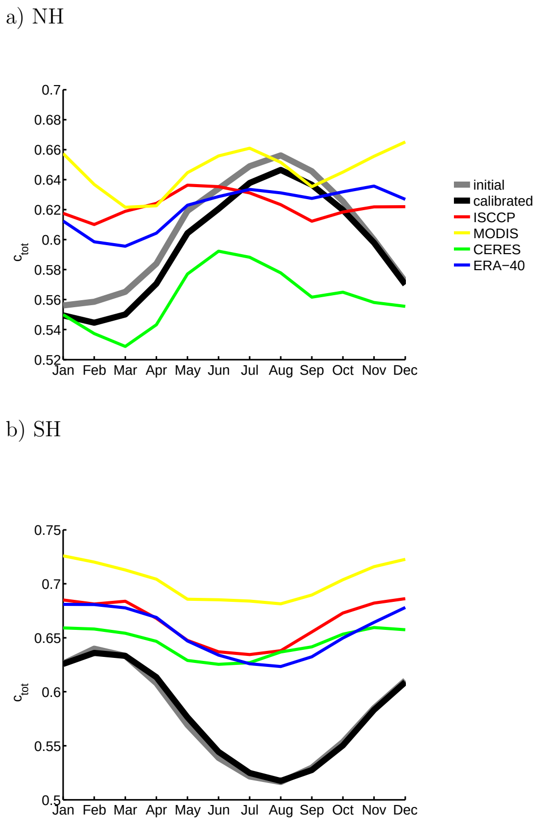

Fig. 1. Total cloud amounts (fraction) averaged over the Northern and Southern Hemispheres (**a** and **b** respectively) for the model with initial guess and calibrated parameter sets (gray and black lines correspondingly) as well as for the ISCCP, MODIS, CERES, and ERA-40 data sets (red, yellow, green, and blue curves correspondingly).

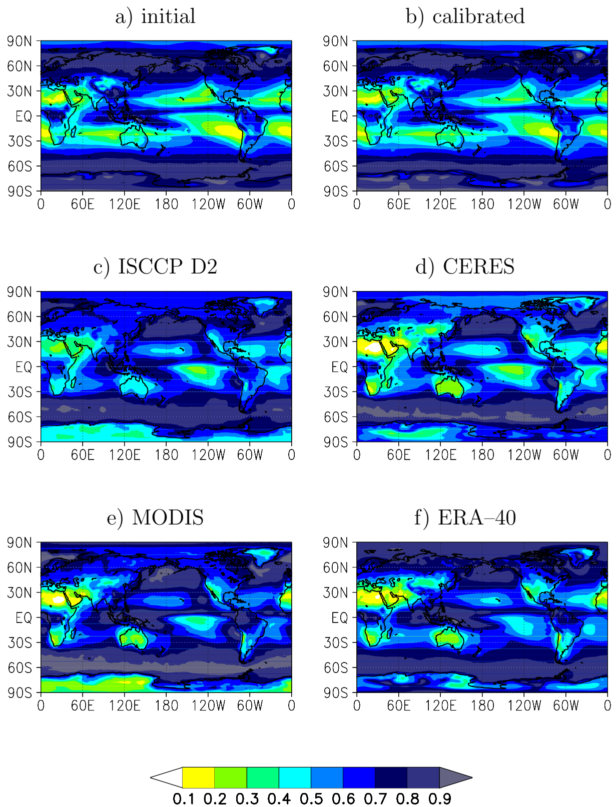

Fig. 2. Annual mean modelled total cloud amount (fractions) for initial and calibrated parameter sets (**a** and **b** correspondingly) in comparison to the ISCCP D2, CERES, MODIS, and ERA-40 climatologies (**c**, **d**, **e**, and **f** respectively).

GMDD
6, 3241–3287, 2013

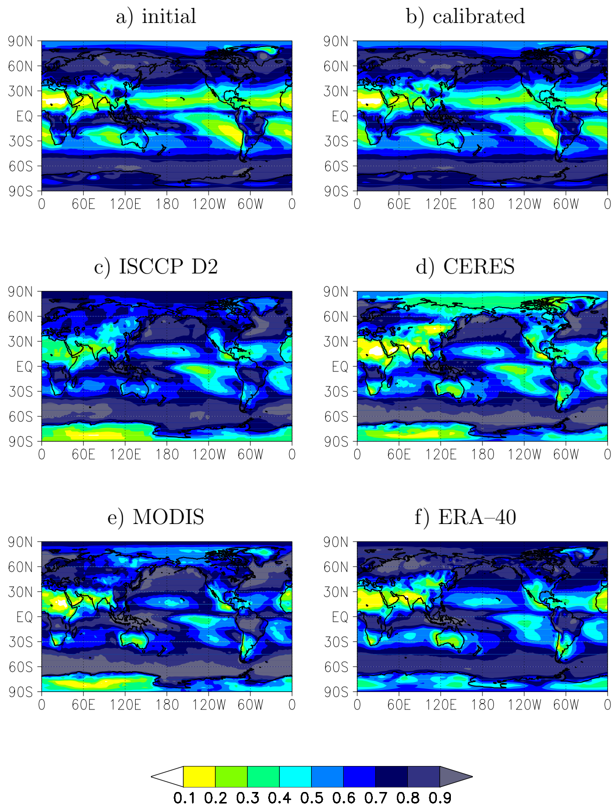

Fig. 3. Similar to Fig. 2 but for January.

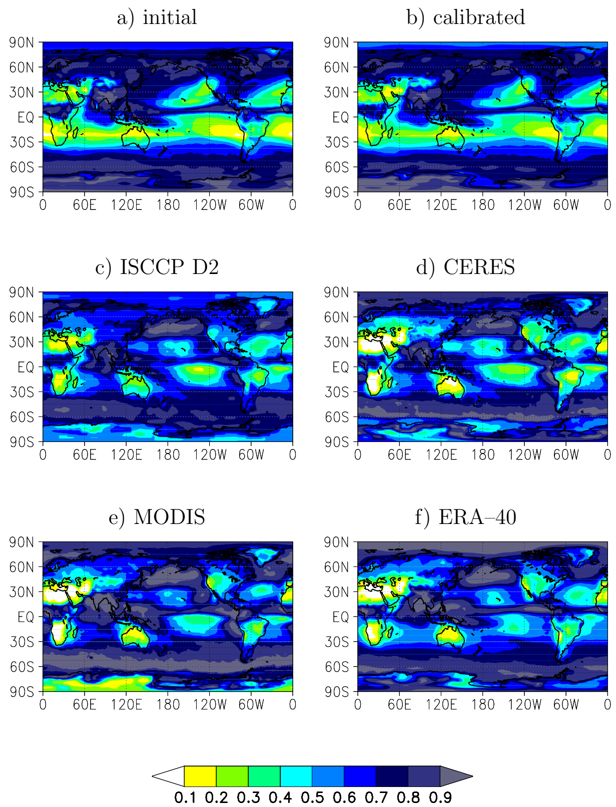

Fig. 4. Similar to Fig. 2 but for July.

GMDD
6, 3241–3287, 2013

Scheme for cloudiness and precipitation for EMICs

A. V. Eliseev et al.

Title Page
Abstract Introduction
Conclusions References
Tables Figures
◀◀ ▶▶
◀ ▶
Back Close
Full Screen / Esc
Printer-friendly Version
Interactive Discussion

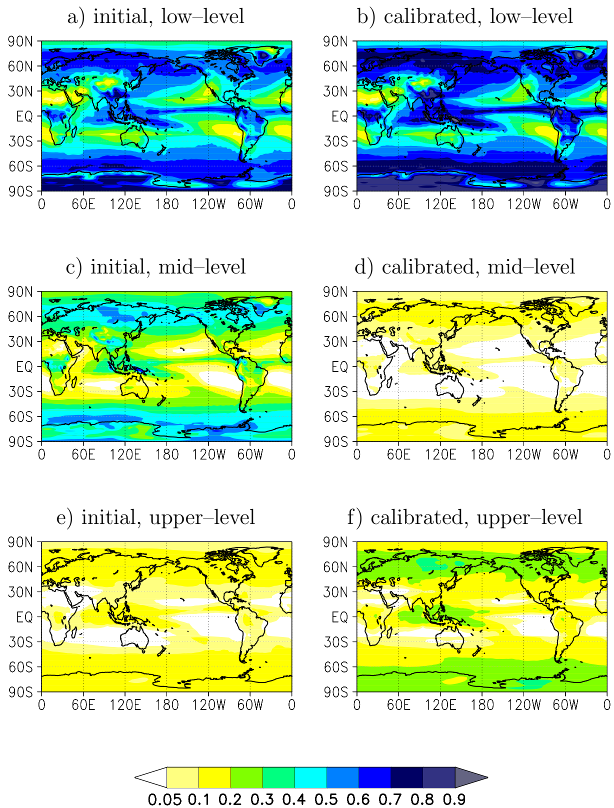

Fig. 5. Annual mean low-level cloud amount $c_l \equiv c_{sl} + c_{co}$ (**a** and **b**), mid-level cloud amount $c_m \equiv c_{sm}$ (**c** and **d**), and upper-level cloud amount $c_h \equiv c_{sh}$ (**e** and **f**) for the model versions with initial (**a**, **c** and **e**) and calibrated (**b**, **d** and **f**) parameter sets. The units are fractions.

GMDD
6, 3241–3287, 2013

Scheme for cloudiness and precipitation for EMICs

A. V. Eliseev et al.

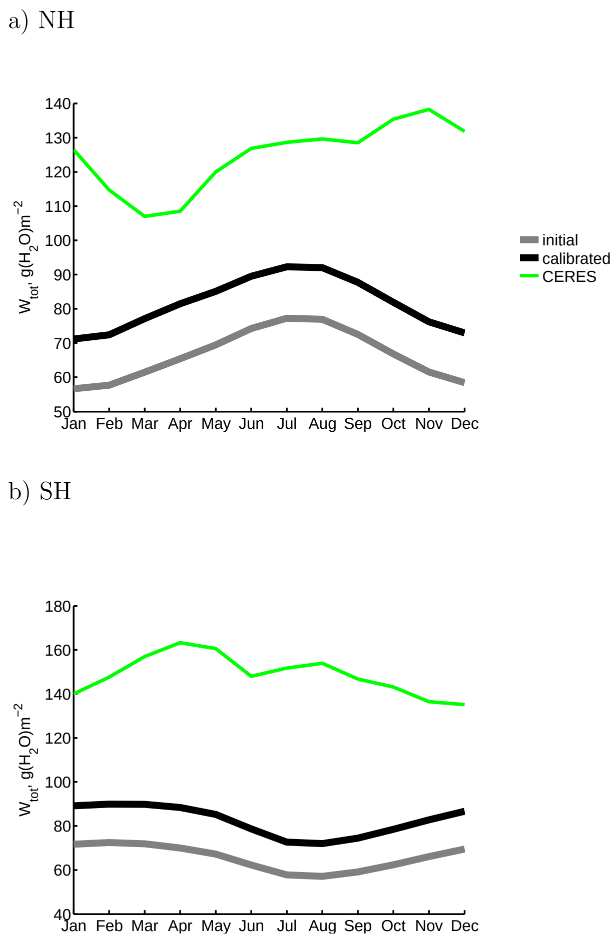

Fig. 6. Cloud water path ($g(H_2O)\,m^{-2}$) averaged over the Northern and Southern Hemispheres (**a** and **b** respectively) for the model with initial and calibrated parameter sets (gray and black lines correspondingly) as well as for the CERES data set (green).

GMDD
6, 3241–3287, 2013

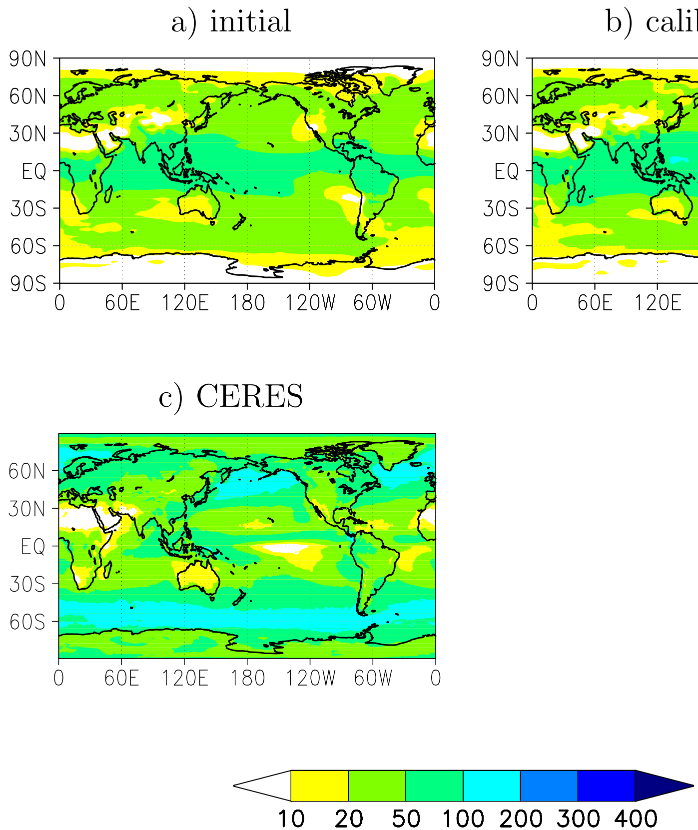

Fig. 7. Annual mean modelled total cloud water path ($g(H_2O)\,m^{-2}$) for initial and calibrated parameter sets (**a** and **b** correspondingly) in comparison to the CERES climatology **(c)**.

GMDD
6, 3241–3287, 2013

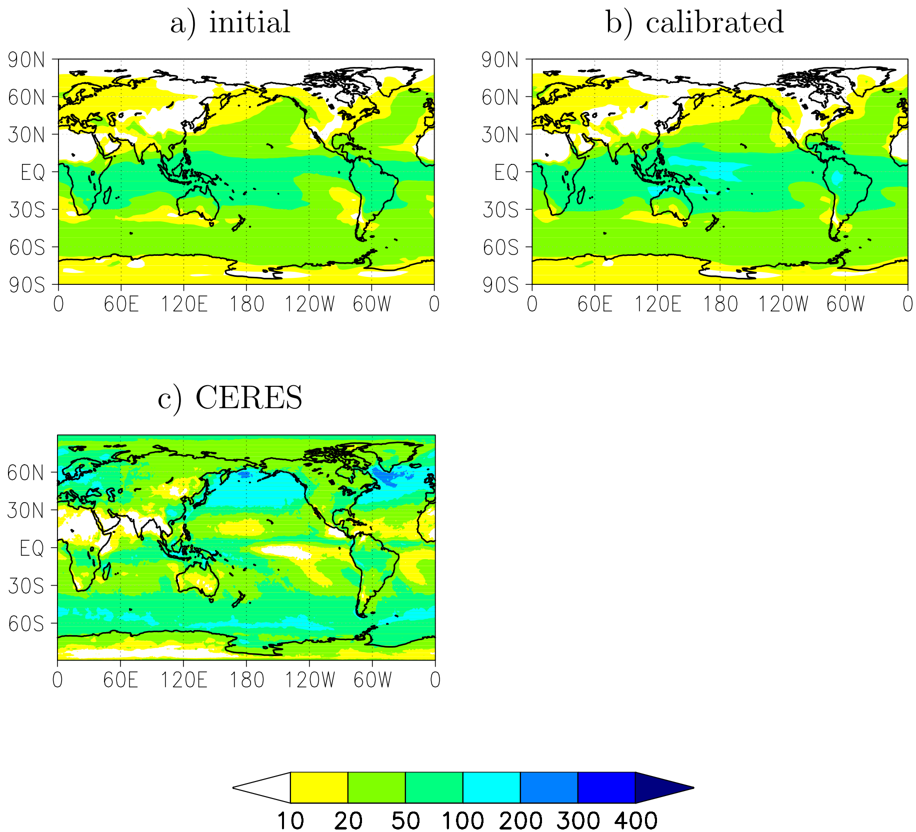

Fig. 8. Similar to Fig. 7 but for January.

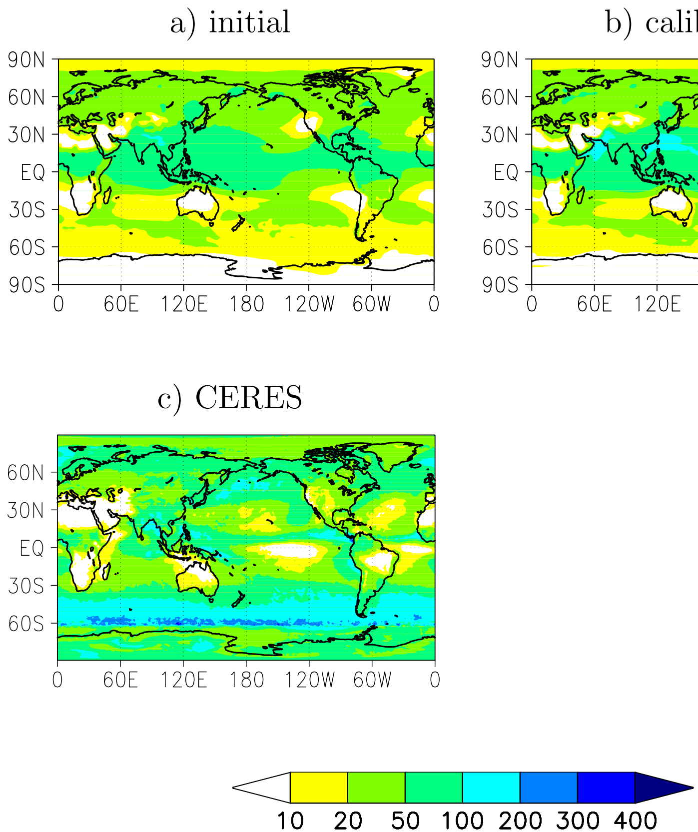

Fig. 9. Similar to Fig. 7 but for July.

GMDD
6, 3241–3287, 2013

Scheme for cloudiness and precipitation for EMICs

A. V. Eliseev et al.

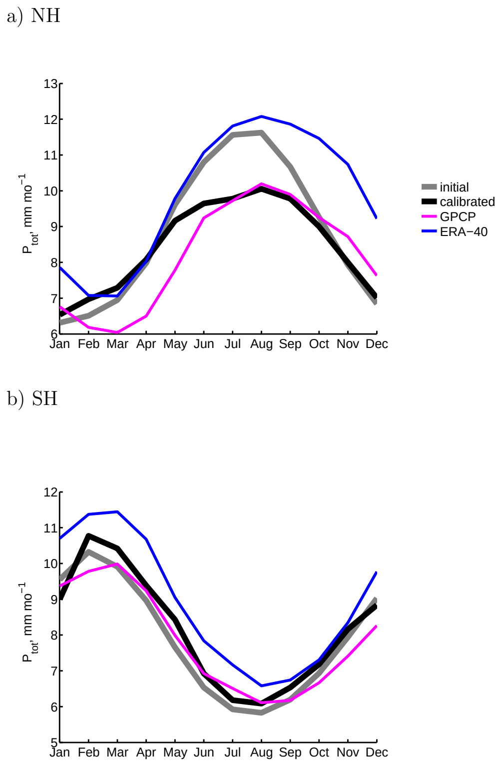

Fig. 10. Total precipitation (cm yr^{-1}) averaged over the Northern and Southern Hemispheres (**a** and **b** respectively) for the model with standard and calibrated parameter sets (gray and black lines correspondingly) as well as for the GPCP and ERA-40 data sets (magenta and blue curves correspondingly).

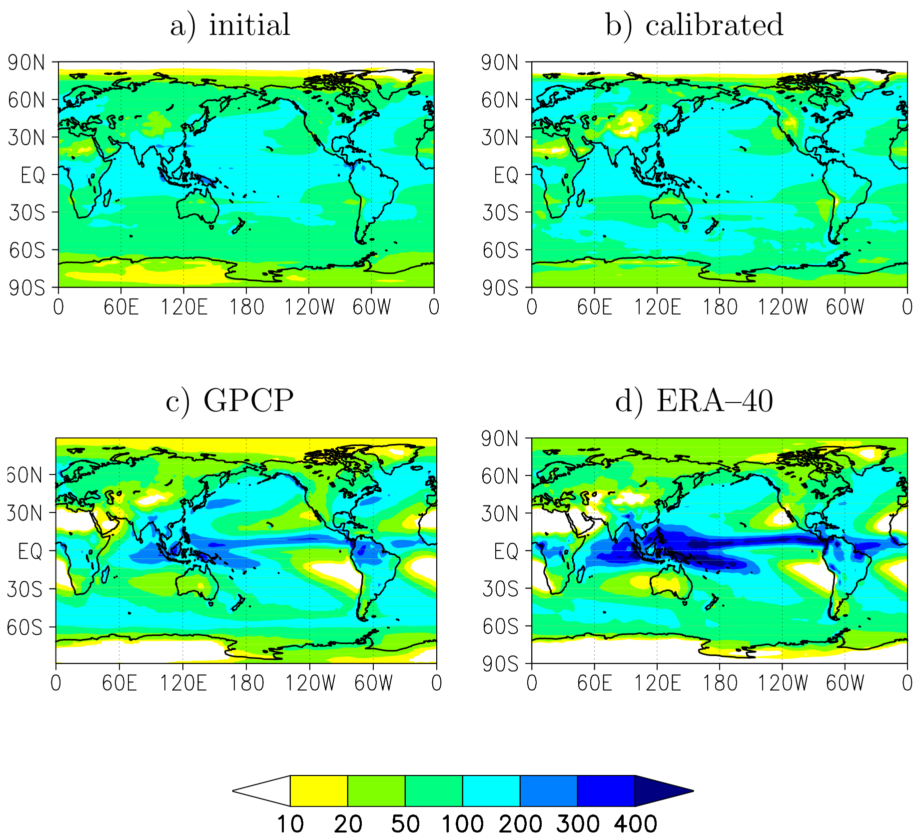

Fig. 11. Annual modelled total precipitation ($cm\,yr^{-1}$) for initial and calibrated parameter sets (**a** and **b** correspondingly) in comparison to the GPCP and ERA-40 climatologies (**c** and **d**).

GMDD
6, 3241–3287, 2013

Scheme for cloudiness and precipitation for EMICs

A. V. Eliseev et al.

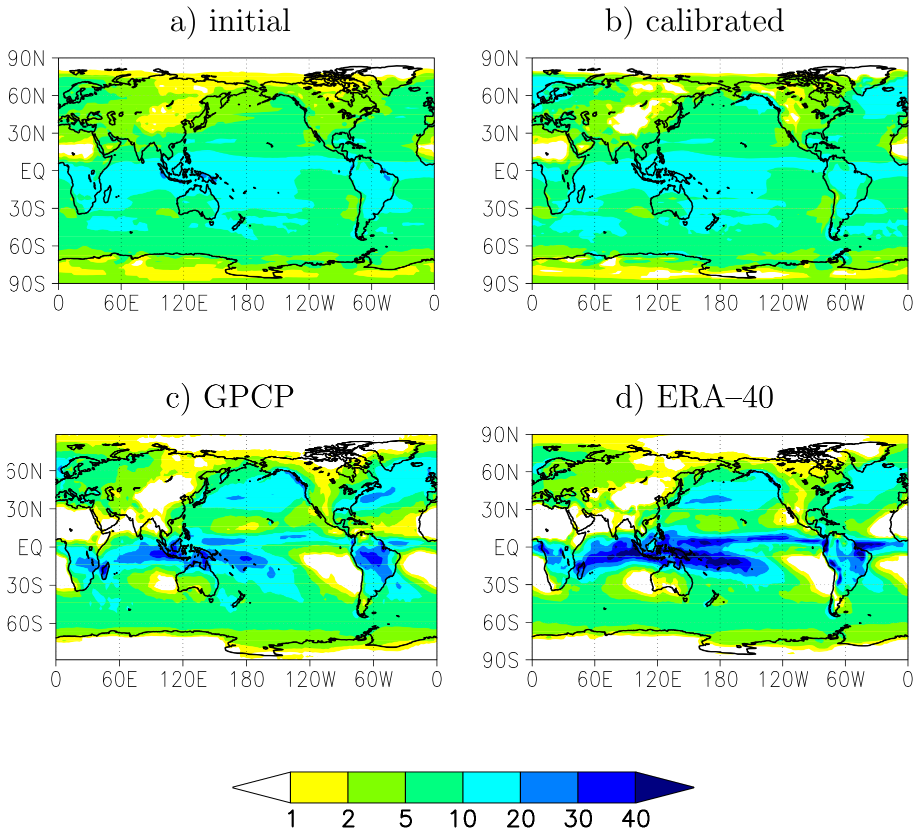

Fig. 12. Similar to Fig. 11 but for January total precipitation (cm mo^{-1}).

GMDD
6, 3241–3287, 2013

Scheme for cloudiness and precipitation for EMICs

A. V. Eliseev et al.

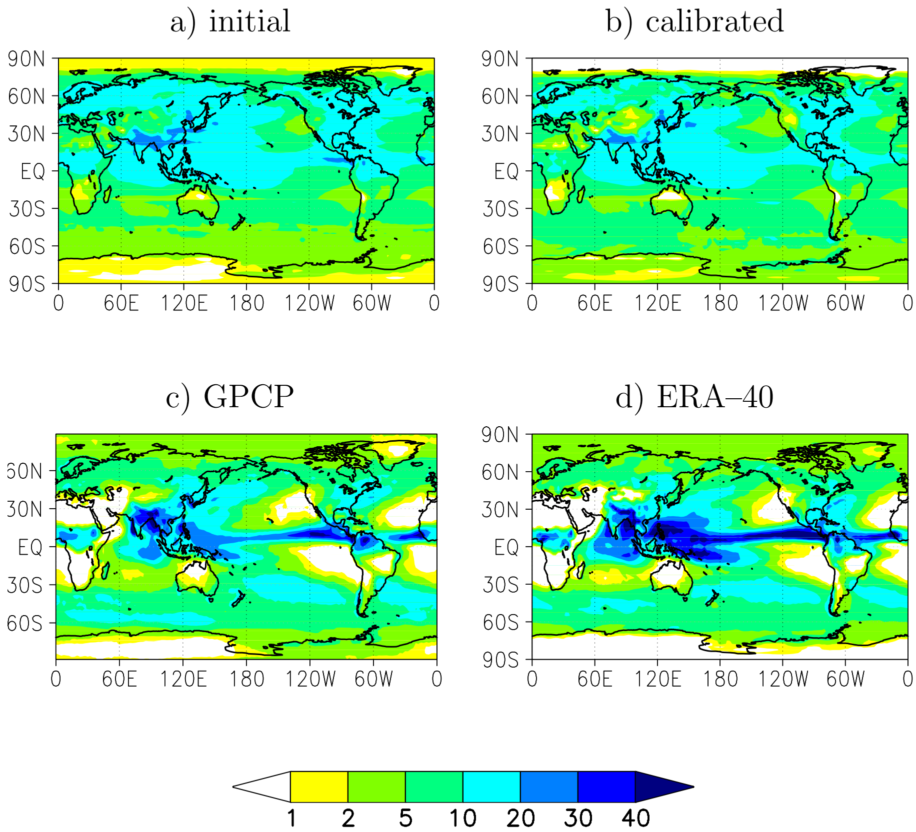

Fig. 13. Similar to Fig. 12 but for July.

GMDD

6, 3241–3287, 2013